Radiography 31 (2025) 112–117

Contents lists available at ScienceDirect

Radiography

journal homepage: www.elsevier.com/locate/radi

Accuracy of deep learning-based attenuation correction in ^{99m}Tc-GSA SPECT/CT hepatic imaging

M. Miyai [a, b, *], R. Fukui [c], M. Nakashima [d], D. Hasegawa [a, e], S. Goto [c]

[a] Department of Radiological Technology, Graduate School of Health Sciences, Okayama University, 2-5-1 Shikata-cho, Kita-ku, Okayama-Shi, Okayama 700-8558, Japan
[b] Department of Radiology, Kawasaki Medical School General Medical Center, 2-6-1 Nakasange, Kita-ku, Okayama-shi, Okayama 700-8505, Japan
[c] Department of Radiological Technology, Faculty of Health Sciences, Okayama University, 2-5-1 Shikata-cho, Kita-ku, Okayama-Shi, Okayama 700-8558, Japan
[d] Division of Radiological Technology, Okayama University Hospital, 2-5-1 Shikata-cho, Kita-ku, Okayama-Shi, Okayama 700-8558, Japan
[e] Department of Radiological Technology, Faculty of Health Science, Kobe Tokiwa University, 2-6-2 Otani-cho, Nagata-ku, Kobe, Hyogo 653-0838, Japan

ARTICLE INFO

Article history:
Received 3 July 2024
Received in revised form
7 October 2024
Accepted 4 November 2024

Keywords:
^{99m}Tc-GSA SPECT/CT
Deep learning
Attenuation correction
Pseudo CT
Generative adversarial network

ABSTRACT

Introduction: Attenuation correction (AC) is necessary for accurate assessment of radioactive distribution in single photon emission computed tomography (SPECT). The method of computed tomography-based AC (CTAC) is widely used because of its accuracy. However, patients are exposed to radiation during CT examination. The purpose of this study was to generate pseudo CT images for AC from non-AC SPECT images using deep learning and evaluate the effect of deep learning-based AC in ^{99m}Tc-labeled galactosyl human serum albumin SPECT/CT imaging.
Methods: A cycle-consistent generative network (CycleGAN) was used to generate pseudo CT images. The test cohort consisted of each one patient with normal and abnormal liver function. SPECT images were reconstructed without AC ($SPECT_{NC}$), with conventional CTAC ($SPECT_{CTAC}$), and with deep learning-based AC ($SPECT_{GAN}$). The accuracy of each AC was evaluated using the total liver count and the structural similarity index (SSIM) of $SPECT_{CTAC}$ and $SPECT_{GAN}$. The coefficient of variation (%CV) was used to assess uniformity.
Results: The total liver counts in $SPECT_{GAN}$ were significantly improved over those in $SPECT_{NC}$ and differed from those of $SPECT_{CTAC}$ by approximately 7 % in both patients. The %CV in $SPECT_{CTAC}$ and $SPECT_{GAN}$ were significantly lower than those in $SPECT_{NC}$. The mean SSIM in $SPECT_{CTAC}$ and $SPECT_{GAN}$ for patients with normal and abnormal liver functions were 0.985 and 0.977, respectively.
Conclusions: The accuracy of AC with a deep learning-based method was similarly performed as the conventional CTAC. Our proposed method used only non-AC SPECT images for AC, which has great potential to reduce patient exposure by eliminating CT examination.
Implications for practice: AC of ^{99m}Tc-GSA was achieved using pseudo CT images generated with CycleGAN. Further studies on changing liver morphology and various hepatic diseases are recommended.

Introduction

Evaluation of liver function is important to prevent post-operative liver failure in patients undergoing hepatic resection. The index of ^{99m}Tc-labeled galactosyl human serum albumin (^{99m}Tc-GSA) closely correlated with indocyanine green retention at 15 min (ICGR15).[1] Many reports have shown that ^{99m}Tc-GSA scintigraphy is a useful diagnostic imaging for the assessment of liver function and reserves.[2,3] Single photon emission computed tomography (SPECT) can be used as a quantitative index for evaluating regional liver function reserve and a simulation of preoperative liver surgery.[4,5] They are evaluated using liver counts, which are the amount of tracer accumulation in the liver. However, the liver is a large organ, and the effects of gamma-ray attenuation are expected to vary significantly between the surface and the center of the body. Therefore, attenuation correction (AC) is necessary to accurately determine the radioactivity distributions of ^{99m}Tc-GSA. The computed tomography-based attenuation correction (CTAC)

* Corresponding author. Department of Radiological Technology, Graduate School of Health Science, Okayama University, 2-5-1 Shikata-cho, Kita-ku, Okayama-Shi, Okayama 700-8558, Japan.
E-mail address: miya0210@hp.kawasaki-m.ac.jp (M. Miyai).

https://doi.org/10.1016/j.radi.2024.11.002
1078-8174/

method is widely employed for AC because it is simple and highly accurate.[6] However, the patient radiation dose associated with computed tomography (CT) imaging is a serious concern.[7,8]

Deep learning technologies have recently shown multiple applications in medical imaging. Conventional neural networks (CNN), which are widely recognized as a leading deep learning technology, are used to improve image quality.[9] Generative adversarial networks (GAN) have been proposed as excellent unsupervised learning methods and applied to image-transformation techniques based on deep learning.[10,11] Salimi et al.[12] proposed a method to acquire pseudo CT images from non-AC positron emission tomography (PET) by using deep neural networks and employed these CT images for AC in whole-body PET imaging. Many other reports have also described AC using deep learning-based methods.[13–15] Our previous study reported that ^{99m}Tc-GSA SPECT/CT hepatic image quality was significantly improvement with deep learning-based AC, however this study was performed using a liver phantom.[16] To the best of our knowledge, no studies have examined ^{99m}Tc-GSA SPECT/CT hepatic imaging with deep learning-based AC using clinical data.

In this study, we generated pseudo CT images from non-AC SPECT images using a GAN and proposed a deep learning-based AC method for ^{99m}Tc-GSA SPECT/CT hepatic imaging using these pseudo CT images in clinical cases. The SPECT images corrected by pseudo CT and the conventional CTAC method were compared by estimating the total count of the whole liver, similarity, and uniformity in patients with normal and abnormal liver function.

Materials and methods

Patients

The training data consisted of the images obtained from 40 patients (age, 56–88 years; mean age, 70.4 ± 7.6 years; 26 men and 14 women) who underwent ^{99m}Tc-GSA imaging from April 2020 to March 2022. The patients' liver function was normal (HH15 $\leq$ 0.51 and LHL15 $\geq$ 0.95).[17] HH15 and LHL15 are indices calculated from ^{99m}Tc-GSA dynamic planner imaging.[18]

The test data were prepared randomly one patient from the normal and abnormal groups: one male patient with normal liver function (age, 76 years; HH15 = 0.49; LHL15 = 0.96; preoperative assessment of cholangiocarcinoma) and one male patient with abnormal liver function (age, 73 years; HH15 = 0.61; LHL15 = 0.86; alcoholic cirrhosis) were prepared. The training and test data showed no large tracer defects due to hepatocellular carcinoma and geometry changes due to hepatectomy or advanced cirrhosis. Ethical approval for this study was obtained from the ethics committee of our university (approval number K2209-007) , and the requirement for informed consent was waived because of the retrospective nature of the study.

SPECT/CT imaging

SPECT was performed using a dual-head detector SPECT/CT system (GE Healthcare, Waukesha, WI, USA) equipped with a low-energy high-resolution collimator. SPECT data were acquired for 15 s/projection using a 128 × 128 matrix (4.4 mm/pixel), an acquisition arc of 360°, and 60 projections. The acquisition energy window was set to 140 keV ±10 % for the main window and 122 keV ±7 % for the sub-window.

The CT images for CTAC were obtained using the same SPECT/CT system. The CT scan parameters were as follows: tube voltage, 120 kV; auto exposure control; rotation time, 0.5 s; beam pitch, 1.375; field of view, 500 mm; slice thickness, 5 mm; and matrix, 512 × 512. CT image voxel values were transformed into linear attenuation coefficients for photon energy, and attenuation maps were created.

The SPECT image reconstruction was performed using the three-dimensional ordered subset expectation maximization (3D-OSEM) method with a Xeleris 3.1 processing system (GE Healthcare). The number of iterations was 10, and the subset was 10.[19] A gaussian filter (full width at half maximum, 14 mm) was used as a prefilter. Zeintl et al.[20] reported that AC, scatter correction (SC), and resolution recovery correction (RR) were provided highly accurate radioactivity distributions. Therefore, AC using CT images, SC using a dual-energy window, and RR were applied to the reconstructed images. SPECT images without correction ($SPECT_{NC}$), with conventional CTAC method ($SPECT_{CTAC}$), and with deep learning-based AC method ($SPECT_{GAN}$) were reconstructed for evaluation.

Image transformation techniques with deep learning

1) GAN

GAN is image transformation techniques based on deep learning.[10] GAN consists of two models (a generator and a discriminator) that are trained simultaneously. The purpose of the generator is to create samples that accurately reflect the characteristics of the training data and thus make the resulting samples indistinguishable from the training data. On the other hand, the purpose of the discriminator is to determine whether a particular sample is true or false. These two models repeat those operations to create a highly accurate network. The result is the created images with a generator that are difficult to distinguish from the real images.

2) CycleGAN

In this study, we used a cycle-consistent generative adversarial network (CycleGAN) model, which is an unsupervised image-to-image transformation technique.[11] Conventional image transformation techniques require paired dataset. However, CycleGAN does not require a paired dataset. An outline of CycleGAN and flowchart of the process for acquiring pseudo CT images is shown in Fig. 1. CycleGAN contains two generators (SPECT-to-CT and CT-to-SPECT) and the associated adversarial discriminators. CycleGAN learns the transformation from $SPECT_{NC}$ to real CT images and the inverse transformation from real CT images and $SPECT_{NC}$ in parallel. A series of learning steps is performed for the number of epochs, resulting in a model that converts a SPECT image to a CT image. After training the model, the generation of pseudo CT images for evaluation is performed by inputting the $SPECT_{NC}$ image into the trained model.

3) Development environment of CycleGAN

The CycleGAN network was implemented using Python 3.6 (Python Software Foundation, Wilmington, DE, USA) as the programming language and PyTorch (Meta Platforms Inc., Menlo Park, CA, USA) as the framework for constructing the network. The networks were trained using Adaptive Moment Estimation. An initial learning rate of 10^{-3} was used for training. The generator was trained using the weights for the adversarial loss ($\lambda_{adv} = 10.0$) and the cycle consistency loss ($\lambda_{cycle} = 10.0$), respectively. The number of epochs was 100 because the loss was converged. The batch size was set to one to avoid mode collapse.[21] Approximately 30 SPECT and CT images of the liver were acquired for each patient. Thus, the training dataset consisted of approximately 1200 images.

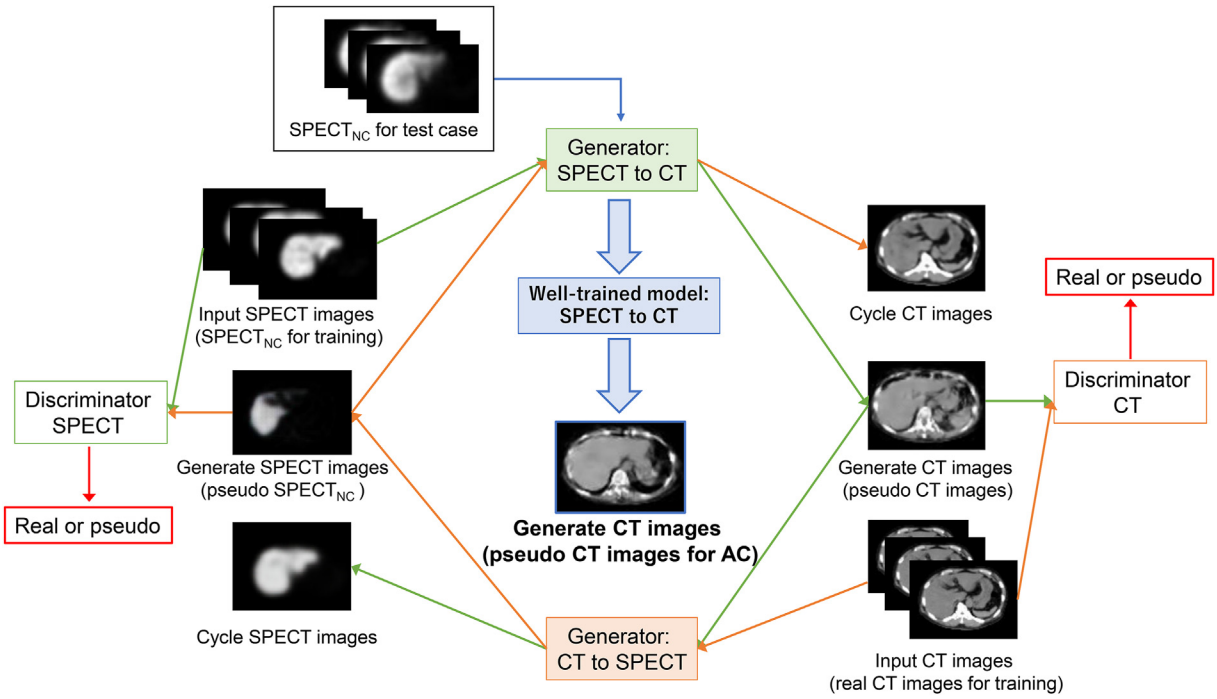

Figure 1. Outline of CycleGAN and flowchart of the process for acquiring the pseudo CT images. CycleGAN learns the domain relationships between SPECT and CT images. Two generators (SPECT-to-CT and CT-to-SPECT) were used to transform the training datasets and generate pseudo images. Subsequently, the generated images were evaluated using the two discriminators. This procedure was repeated to obtain a well-trained model. Finally, the pseudo CT images for AC were predicted using this model.

Evaluation

1) Structural similarity

The total liver counts were used to assess the accuracy of AC. The regions of interest (ROIs) manually created by referring to real CT images on the entire liver for SPECT$_{NC}$, SPECT$_{CTAC}$ and SPECT$_{GAN}$ (Fig. 2(a)). Additionally, the structural similarity index (SSIM) was used to compare the similarities between SPECT$_{CTAC}$ and SPECT$_{GAN}$. SSIM is an index for perceptual structural distortion and is a conventional and popular metric in image processing.[22] The formula used to calculate SSIM was as follows:

$$SSIM = \frac{\left(2\mu_x\mu_y + C_1\right)\left(2\sigma_{xy} + C_2\right)}{\left(\mu_x{}^2 + \mu_y{}^2 + C_1\right)\left(\sigma_x{}^2 + \sigma_y{}^2 + C_2\right)} \quad (1)$$

where μ_x and μ_y, σ_x, σ_y and σ_{xy} are the local means, standard deviations, and cross-covariance of image x ($SPECT_{CTAC}$) and y ($SPECT_{GAN}$), respectively. $C_1 = (K_1L)^2$, $C_2 = (K_2L)^2$, K_1 and K_2 are constants with values of 0.01 and 0.03, respectively, and L denotes the pixel value range of the image. An SSIM value close to 1 corresponds to an ideal agreement between two images, whereas a lower SSIM value indicates a discrepancy between the two images.

2) Uniformity

The coefficient of variation (%CV) was calculated as an index of liver uniformity.[23] Therefore, as shown in Fig. 2(b), three ROIs were placed in the right and left lobes (three slices at the center) on SPECT$_{NC}$, SPECT$_{CTAC}$, and SPECT$_{GAN}$, respectively.[24] The ROI size was 37 pixels. The %CV values were calculated using the following equation:

$$\%CV = \frac{SD}{mean} \times 100\ (\%) \quad (2)$$

where *mean* is the mean count and *SD* is the standard deviation. Data were analyzed by using One-Way analysis of variance and

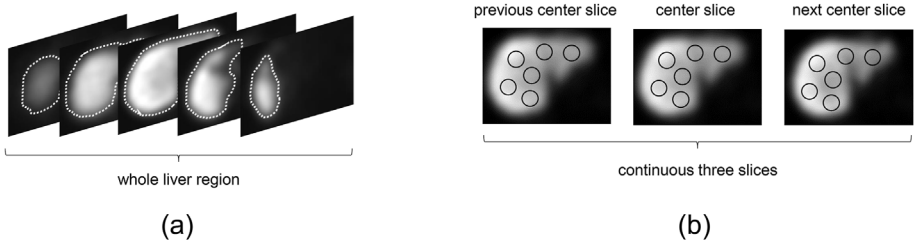

Figure 2. Regions of interest (ROIs) used in the calculation of the liver total counts and the %CV values. The %CV evaluation was performed to assess image uniformity. (a) ROIs were set in the whole liver regions of SPECT$_{NC}$, SPECT$_{CTAC}$, and SPECT$_{GAN}$, and the liver total counts were evaluated to determine the accuracy of AC. (b) 18 ROIs were located on the liver regions of SPECT$_{NC}$, SPECT$_{CTAC}$, and SPECT$_{GAN}$.

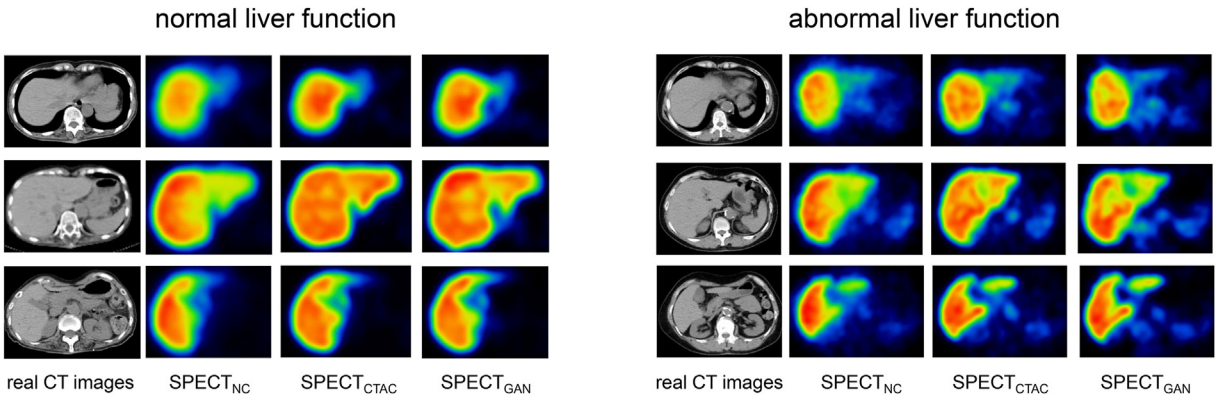

Figure 3. SPECT$_{NC}$, SPECT$_{CTAC}$ and SPECT$_{GAN}$ images in cases with normal and abnormal liver function. In both cases, SPECT$_{CTAC}$ and SPECT$_{GAN}$ showed significant improvements in central liver counts in comparison with SPECT$_{NC}$.

Bonferroni post-hoc test ($p < 0.05$). The statical analysis was performed using SPSS software (SPSS Inc., Chicago, IL, USA).

The evaluation indices were acquired using Prominence Processor version 3.1[25] (released by Japanese Society of Radiological Technology subgroup; Nuclear medicine Section) and ImageJ software (National Institutes of Health, Bethesda, Maryland, USA).

Results

1) Structural similarity

As shown in Fig. 3, we confirmed the counts in the deep liver regions after AC in SPECT$_{CTAC}$ and SPECT$_{GAN}$. Fig. 4 showed the total counts in each SPECT images. Considering the total counts in SPECT$_{CTAC}$ as the reference, the total counts in SPECT$_{NC}$ and SPECT$_{GAN}$ in the patient with normal liver function were 59 % and 6.5 % lower, respectively (Fig. 4(a)). Similarly, the total counts in SPECT$_{NC}$ and SPECT$_{GAN}$ in the patient with abnormal liver function were 61 % and 7.2 % lower than the reference value, respectively (Fig. 4(b)).

Fig. 5 showed the pseudo CT images of the patient with normal liver function. The liver, spine, ribs, and aorta were well-generated. However, other organs (stomach, intestinal tract, and spleen) were not well-generated. Similar results were observed in the patient with abnormal liver function.

The mean SSIM for SPECT$_{CTAC}$ and SPECT$_{GAN}$ in the patient with normal liver function was 0.985 ± 0.00189, while the mean SSIM in the patient with abnormal liver function was 0.977 ± 0.00191.

2) Uniformity

Considering the %CV in SPECT$_{NC}$ as the reference, the %CV values in SPECT$_{CTAC}$ and SPECT$_{GAN}$ for the patient with normal liver function were 36 % and 31 % lower, respectively (Fig. 6(a)). Similarly, the %CV values in SPECT$_{CTAC}$ and SPECT$_{GAN}$ for the patient with abnormal liver function were 27 % and 25 %, respectively (Fig. 6(b)). The %CV value in the patient with abnormal liver function was slightly higher than that in the patient with normal liver function.

Discussion

In this study, we employed the CycleGAN network to generate the pseudo CT images from SPECT$_{NC}$ and finally obtained SPECT$_{GAN}$. We then evaluated the accuracy of AC in each reconstructed SPECT images (SPECT$_{NC}$, SPECT$_{CTAC}$ and SPECT$_{GAN}$) using the total counts, SSIM, and %CV values.

In cases with normal and abnormal liver function, the deep liver region counts in SPECT$_{GAN}$ were significantly improved over those in SPECT$_{NC}$. However, the total counts in SPECT$_{GAN}$ were approximately 7 % lower than those in SPECT$_{CTAC}$. The results were similar to the previous report.[16] One possible reason for this finding may be

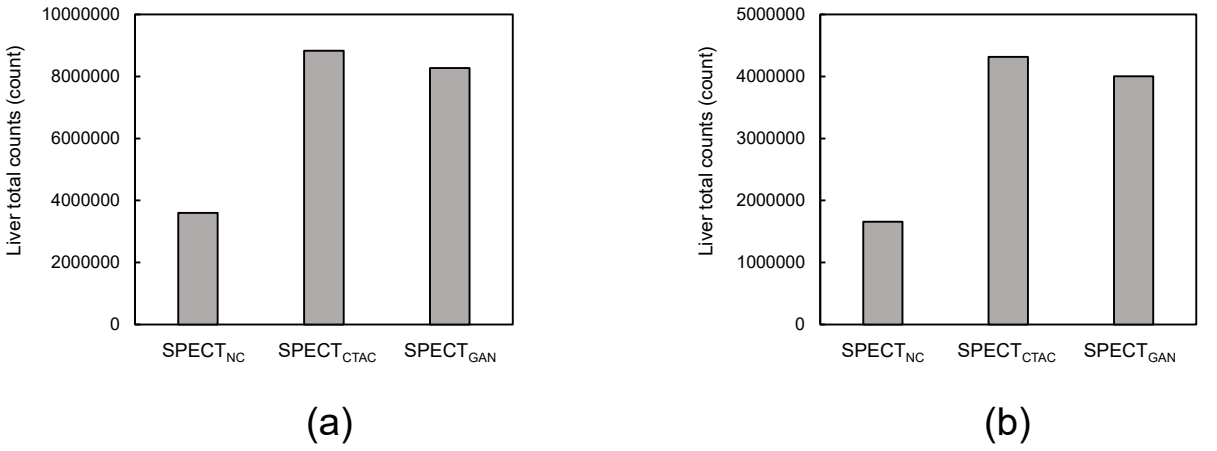

Figure 4. The liver total counts of SPECT$_{NC}$, SPECT$_{CTAC}$, and SPECT$_{GAN}$ in cases with (a) normal and (b) abnormal liver function. In both cases, SPECT$_{CTAC}$ and SPECT$_{GAN}$ exhibit higher values than SPECT$_{NC}$.

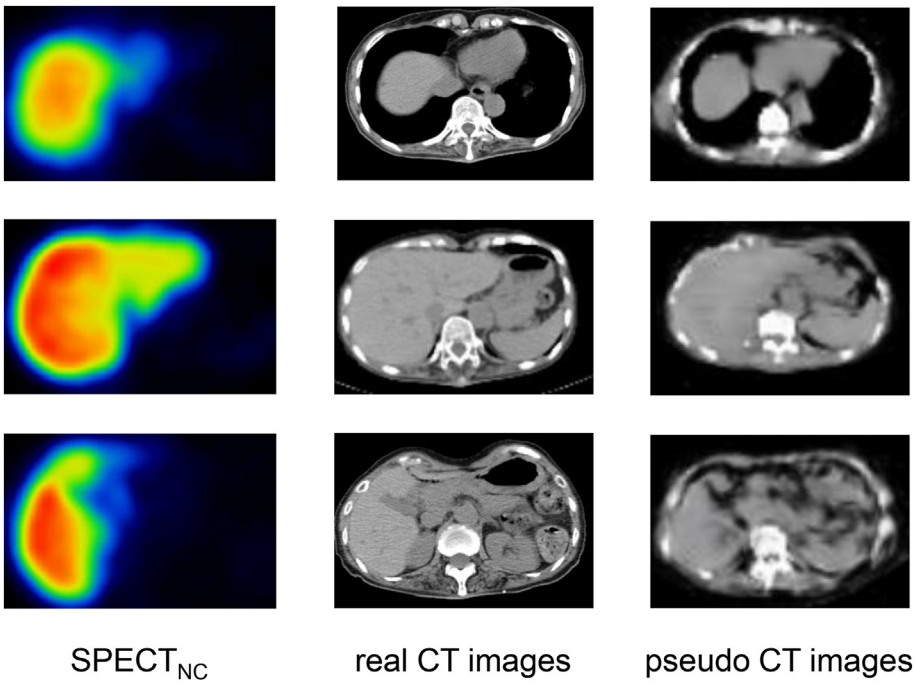

Figure 5. The real CT images and the pseudo CT images in the case with normal liver function. The organs were well-generated with little individual variation in their positions. However, organs with low-contrast signals due to a lack of tracer uptake were difficult to generate.

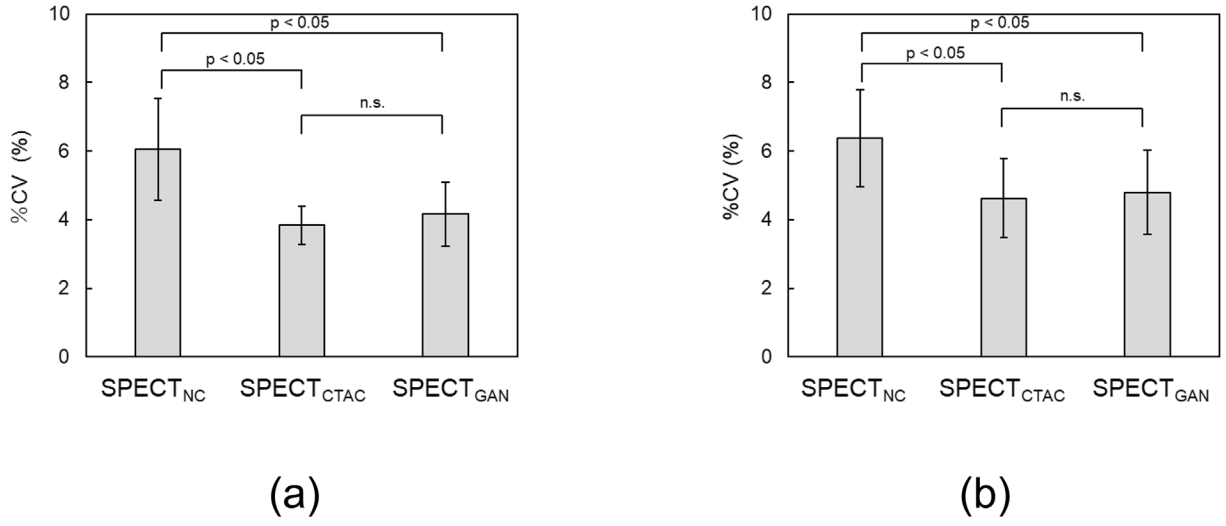

Figure 6. The %CV values of SPECT$_{NC}$, SPECT$_{CTAC}$ and SPECT$_{GAN}$ in cases with (a) normal and (b) abnormal liver function. In both cases, SPECT$_{CTAC}$ and SPECT$_{GAN}$ exhibit lower values than SPECT$_{NC}$. The image uniformities of SPECT$_{CTAC}$ and SPECT$_{GAN}$ are significantly better.

that pseudo CT images did not adequately generate all the organs. Because the pseudo CT images were generated with reference to the accumulation of ^{99m}Tc-GSA in SPECT$_{NC}$, organs in regions without radioisotope uptake were assigned structures predicted from the training datasets. Dong et al.[13] reported that a low-contrast region is a challenge in accurately predicting CT images using the CycleGAN model. However, the difference in the total counts of SPECT$_{CTAC}$ and SPECT$_{GAN}$ was small, and the slight structural mismatch between real CT images and pseudo CT images did not significantly affect the accuracy of AC. LaCroix et al.[26] reported that despite the inaccurate estimation of the attenuation maps generated from CT images, the reconstructed SPECT images provided estimates of radioactivity concentrations with few errors and artifacts. In addition, a bilinear model was used for CTAC in this study, and small differences in CT values, such as organ mismatches, are not expected to result in large differences in the attenuation coefficients.[27]

The mean SSIM indices for SPECT$_{CTAC}$ and SPECT$_{GAN}$ were 0.985 and 0.977 in the patients with normal and abnormal liver function, respectively. The SSIM values were close to 1, indicating that the SPECT$_{CTAC}$ and SPECT$_{GAN}$ were similar. Yang et al.[14] reported that the SSIM of SPECT images with CTAC and deep learning-based AC was 0.993. They used a semiconductor SPECT system with a high resolution. We believe that improving the quality of the training dataset using a high resolution and sensitivity SPECT system would produce more similar SPECT images, resulting in a SSIM closer to 1.

Because the %CV values of $SPECT_{CTAC}$ and $SPECT_{GAN}$ were approximately 30 % lower than those of $SPECT_{NC}$, this result indicates improved uniformity. One of the main reasons for this finding is the RR correction. A previous study showed that a reconstruction method with RR improves image uniformity by approximately 30 % in comparison with conventional reconstruction methods without RR.[23] Additionally, the %CV values of the cases with abnormal liver function were slightly higher than those of the cases with normal liver function. Because patients with abnormal liver function showed lower liver accumulation of counts and their findings were affected by statistical variability, the estimated uniformity was poor. However, the results of each our evaluation showed the usefulness of $SPECT_{GAN}$. Our proposed method allows to eliminate the CT scan for the purpose of AC and to adapt the CTAC method with CT-less SPECT system. In this study, we used SPECT/CT system. However, CycleGAN does not require paired images to create a training model. Therefore, in facilities that only have CT-less SPECT system, the SPECT images obtained with that device (non-AC SPECT images) and CT images obtained from separate CT system can be performed our proposed method.

This study had the following limitations. CycleGAN generates CT images by training SPECT image characteristics. In this study, cases with normal liver geometry were used as the test data. Therefore, the applicability of the generated CycleGAN model should be examined in cases of hepatocellular carcinoma with defective the radioactivity distributions of ^{99m}Tc-GSA and in cases of abdominal heterotaxy. Diseases showing specific accumulation patterns of ^{99m}Tc-GSA may require a CycleGAN model generated from training data customized for each disease.

Conclusions

We proposed a deep learning-based AC method to generate the pseudo CT images using non-AC SPECT images in ^{99m}Tc-GSA SPECT/CT hepatic imaging. The accuracy of AC using the proposed method was almost equal to that of conventional CTAC using real CT images. By excluding CT examinations using the proposed method, we believe that the patient radiation dose in ^{99m}Tc-GSA SPECT/CT hepatic imaging could be reduced.

Acknowledgments

The authors are grateful to all the staff members of Okayama University Hospital. This research did not receive any specific grant funding agencies in the public, commercial, or not-for-profit sectors.

References

1. Kawamura H, Kamiyama T, Nakagawa T, Nakanishi K, Yokoo H, Takahara M, et al. Preoperative evaluation of hepatic functional reserve by converted ICGR15 calculated from Tc-GSA scintigraphy. *J Gastroenterol Hepatol* 2008;**23**:1235–41.
2. Kasai M, Ha-kawa S, Aihara T, Ikura S, Nakajima T, Yamanaka N. Establishment and internal validation of a prognostic score for post-hepatectomy liver failure based on functional liver parameters estimated via Tc-99m GSA. *Cureus* 2023;**15**:e42297.
3. Kaibori M, Ha-Kawa SK, Maehara M, Ishizaki M, Matsui K, Sawada S, et al. Usefulness of Tc-99m-GSA scintigraphy for liver surgery. *Ann Nucl Med* 2011;**25**:593–602.
4. Tokorodani R, Sumiyoshi T, Okabayashi T, Hata Y, Noda Y, Morita S, et al. Liver fibrosis assessment using 99 mTc-GSA SPECT/CT fusion imaging. *Jpn J Radiol* 2019;**37**:315–20.
5. Iida M, Yamamoto Y, Katoh H, Taniguchi N, Abe Y, Kumagai K, et al. 99 mTc-GSA scintigraphy for assessing the functional volume ratio of the future liver remnant in the routine practice oh liver resection. *Surg Open Sci.* 2022;**15**:1–8.
6. Bailey DL, Willowson KP. An evidence-based review of quantitative SPECT imaging and potential clinical applications. *J Nucl Med* 2013;**54**:83–9.
7. Sharma P, Sharma S, Ballal S, Bal C, Malhotra A, Kumar R. SPECT-CT in routine clinical practice: increase in patient radiation dose compared with SPECT alone. *Nucl Med Commun* 2012;**33**:926–32.
8. Rausch I, Füchsel FG, Kuderer C, Hentschel M, Bayer T. Radiation exposure levels of routine SPECT/CT imaging protocols. *Eur J Radiol* 2016;**85**:1627–36.
9. Lei Y, Dong X, Wang T, Higgins K, Liu T, Curran WJ, et al. Whole-body PET estimation from low count statistics using cycle-consistent generative adversarial networks. *Phys Med Biol* 2019;**64**:215017.
10. Goodfellow IJ, Pouget-Abadie J, Mirza M, Xu B, Warde-Farley D, Ozair S, et al. Generative adversarial nets. *NIPS 27 proceeding* 2014:2672–80.
11. Zhu JY, Park T, Isola P, Efros AA. Unpaired image-to-image translation using cycle-consistent adversarial networks. *ICCV2017 Conference Proceedings* 2017;**1**:2242–51.
12. Salimi Y, Shiri I, Sanaat A, Zaidi H. Direct generation of pseudo-CT images from non-attenuation/scatter corrected PET images for CT-less attenuation/scatter correction. *J Nucl Med* 2022;**63**:3266.
13. Dong X, Wang T, Lei Y, Higgins K, Liu T, Curran WJ, et al. Synthetic CT generation from non-attenuation corrected PET images for whole-body PET imaging. *Phys Med Biol* 2019;**64**:215016.
14. Yang J, Shi L, Wang R, Liu C, Gullberg G, Seo Y. CT-less attenuation correction in Image space using deep learning for dedicated cardiac SPECT: a feasibility study. *J Nucl Med* 2020;**61**:223.
15. Armanious K, Küstner T, Reimold M, Nikolaou K, La Fougere C, Yang B, et al. Independent brain ^{18}F-FDG PET attenuation correction -using a deep learning approach with Generative Adversarial Networks. *Hellenic J Nucl Med* 2019;**22**:179–86.
16. Masahiro M, Ryohei F, Masahiro N, Goto Sachico. Deep learning-based attenuation correction method in ^{99m}Tc-GSA SPECT/CT hepatic imaging: a phantom study. *Radiol Phys Technol* 2024;**17**:165–75.
17. Sasaki N, Shiomi S, Iwata Y, Nishiguchi S, Kuroki T, Kawabe J, et al. Clinical usefulness of scintigraphy with 99 mTc-galatosyl-human-serum albumin for prognosis of cirrhosis of the liver. *J Nucl Med* 1999;**40**:1652–6.
18. Kotani K, Kawabe J, Higashiyama S, Yoshida A, Kawamura E, Tamori A, et al. Heterogeneous liver uptake of Tc-99m-GSA as quantified through SPECT/CT helps to evaluate the degree of liver fibrosis: a retrospective observational study. *Medicine* 2018;**97**:e11765.
19. Okuda K, Nakajima K, Yamada M, Wakabayashi H, Ichikawa H, Arai H, et al. Optimization of iterative reconstruction parameters with attenuation correction, scatter correction and resolution recovery in myocardial perfusion SPECT/CT. *Ann Nucl Med* 2014;**28**:60–8.
20. Zeintl J, Vija AH, Yahil A, Hornegger J, Kuwert T. Quantitative accuracy of clinical ^{99m}Tc SPECT/CT using ordered-subset expectation maximization with 3-dimensional resolution recovery, attenuation, and scatter correction. *J Nucl Med* 2010;**51**:921–8.
21. Metz L, Poole B, Pfau D, Sohl-Dickstein J. *Unrolled generative adversarial networks*. A conference paper at ICLR, https://arxiv.org/pdf/1611.021693.pdf; 2017.
22. Wang Z, Bovik AC, Sheikh HR, Simoncelli EP. Image quality assessment: from error visibility to structural similarity. *IEEE Trans Image Process* 2004;**13**:600–12.
23. Onishi H, Motomura N, Fujino K, Natsume T, Haramoto Y. Quantitative performance of advanced resolution recovery strategies on SPECT images: evaluation with use of digital phantom models. *Radiol Phys Technol* 2013;**6**:42–53.
24. Nakamura Y, Tomiguchi S, Tanaka M. Reliability and advantages of using non-uniform Chang's attenuation correction method using a CT-based attenuation coefficient map in ^{99m}Tc-GSA SPECT/CT hepatic imaging. *EJNMMI Phys.* 2015;**2**:17.
25. Maeda H, Yamaki N, Azuma M. Development of the software package of the nuclear medicine data processor for education and research. *Nihon Hoshasen Gijutsu Zasshi* 2012;**68**:299–306.
26. LaCroix KJ, Tsui BMW, Hasegawa BH, Brown JK. Investigation of the use of X-ray CT images for attenuation compensation in SPECT. In: *Proceedings of nuclear science symposium & medical imaging conference*; 1994. p. 1169–73.
27. Patton JA, Turkington TG. SPECT/CT physical principles and attenuation correction. *J Nucl Med Technol* 2008;**36**:1–10.